Magnetic properties of chromium chalcogenide spinels: $Cd_{1-x}Ag_xCr_2Se_4$ and $Hg_{1-x}Ag_xCr_2Se_4$

J. M. Ferreira
Departamento de Física, Universidade Federal de Pernambuco, 50670-901 Recife-PE, Brazil

M. D. Coutinho-Filho
Departamento de Física and Laboratório de Física Teórica e Computacional, Universidade Federal de Pernambuco, 50670-901 Recife-PE, Brazil

(Received 11 August 1995; revised manuscript received 18 July 1996)

The effect of Cr ions of different valences (Cr^{2+}, Cr^{3+}, and Cr^{4+}) on the magnetic anisotropy and ferromagnetic resonance (FMR) linewidth in ferromagnetic semiconductors, with specific application to the chromium chalcogenide spinels $CdCr_2Se_4$ and $HgCr_2Se_4$ (''as grown and Ag doped''), is studied theoretically and experimentally. We generalize various previous calculations and show that the line shape of the FMR depends on the conductivity, the frequency, and the sample dimension. Crystal-field theory is used to calculate the Cr ions low-lying energy levels and their effect on the magnetic anisotropy and FMR relaxation. In particular, we find that the orbital ground state of the Cr^{2+} ion is a doublet and causes a symmetry breaking of the anisotropy from cubic, at high temperatures, to noncubic at low temperatures. We report FMR data of single crystals of $CdCr_2Se_4$ with 0.1 mole % Ag doped, where this effect is seen. Moreover, several relaxation mechanisms are identified which allow the estimates of exchange fields and microscopic relaxation times of Cr ions in these crystals. [S0163-1829(96)06542-3]

I. INTRODUCTION

The effect of Cr ions of different valences, Cr^{2+}, Cr^{3+}, and Cr^{4+}, on the magnetic anisotropy and ferromagnetic resonance (FMR) linewidth of chromium chalcogenide spinels has been intensively investigated after the discovery[1] of magnetism in these compounds. In particular, $CdCr_2Se_4$ and $HgCr_2Se_4$ exhibit ferromagnetism with high magnetization and relatively high Curie temperatures ($T_C = 130-142$ K for $CdCr_2Se_4$ and 106–120 K for $HgCr_2Se_4$) and if stoichiometrically perfect are electrical insulators. The anisotropy caused by the Cr^{3+} host ions is found[2] to be extremely small and the resonance line very narrow. In addition, however, $CdCr_2Se_4$ and $HgCr_2Se_4$ also exhibit semiconducting behavior[3] due to a lack of stoichiometry (as grown), thermal treatment or intentional doping, and may achieve quite large conductivities. The combination of semiconducting and magnetic properties has been the most attractive feature of these chromium chalcogenide compounds.[4] The wide range of nonstoichiometry leads to a strong composition influence on the physical properties.[5] In particular, it causes the appearance of impurity magnetic ions[6] which manifest in anomalous peaks of the resonance field and of the FMR linewidth along some particular crystallographic directions.

Several studies have been made to identify the impurity magnetic ions responsible for the above-mentioned anomalies. It was suggested by Berger and Pinch[7] that Cr^{2+} ions could be formed to charge compensate for Se^{2-} vacancies and qualitatively explain the variation of anisotropy from sample to sample. However, it has also been suggested[8] that accidental Fe^{2+} impurities are responsible for the anisotropy anomalies, after identification[9] of similar effects in $CdCr_2Se_4$ doped with Fe. On the other hand, in Ag-doped $CdCr_2Se_4$ (Ag^+ substituting for Cd^{2+}), a change in sign of the first anisotropy constant K_1 (from positive to negative) was verified[10] and attributed to the formation of Cr^{4+} ions, which could equally be created to charge compensate for Cd vacancies. Further investigations[11] showed that vacuum annealing of Ag-doped $CdCr_2Se_4$ altered the sign of K_1 (now from negative to positive). This change was ascribed to the formation of Cr^{2+} ions,[11] which occurred as Se vacancies appeared in the crystal, whereas subsequent annealing in Se atmosphere reversed the anisotropy sign as the vacancies filled up, though the value of K_1 (<0) was much less in magnitude than the initial one. The presence of Cr^{4+} ions has also been suggested as responsible for the low-temperature peaks of the FMR linewidth of Ag-doped $CdCr_2Se_4$ (Refs. 10 and 12) and of ''as grown'' $HgCr_2Se_4$,[13,14] as well as to explain[13–16] the negative anisotropy of $HgCr_2Se_4$. It should be mentioned that variations in sign occur[17] depending on the degree of deviation from stoichiometry.

In this paper we present a detailed investigation of the effects of impurity doping and temperature (T) on the FMR line shape, linewidth, and anisotropy on the compounds $Cd_{1-x}Ag_xCr_2Se_4$ and $Hg_{1-x}Ag_xCr_2Se_4$.

In the experiments we have used single crystals grown by the closed tube vapor transport method.[18] From these crystals spherical samples with diameter $\Phi = 0.3–0.8$ mm and a sample in form of a slab with dimensions $1.0\times0.6\times0.2$ mm^3 were made. These samples were mechanically polished using abrasive powder with an average particle size near 0.5 mm and oriented by x-ray diffraction to within 1°. FMR resonance experiments were performed in the 3 cm wavelength range either in a standard FMR apparatus containing a TE_{102} rectangular reflection cavity or in a nonresonant system. The sample is placed in either an evacuated cavity or in a section of a shorted waveguide at an antinode of the rf magnetic field. It is mounted on a thin sapphire rod connected to the cold tip of a Helitran cryostat placed between the pole pieces of a magnet. The external magnetic field was made to lie in

the (110) plane of the crystal, so that FMR data could be collected along the principal crystallographic directions. Resonance curves were obtained in the temperature range 4.2 K to T_C and recorded using a heterodyne receiver to improve the signal-to-noise ratio.

In Secs. II and III we present our main experimental data and discuss several phenomenological aspects. In Sec. IV we discuss the level structures of the Cr^{2+}, Cr^{3+}, and Cr^{4+} ions, and the single-ion contributions to the anisotropy of chalcogenide spinels are calculated in Sec. V. Finally in Sec. VI these results, together with others reported in earlier sections, are used to interpret our experimental data. Conclusions concerning the influence of the sample conductivity on the FMR properties and the microscopic mechanisms underlying the FMR linewidth and magnetic anisotropy are also presented.

II. FMR LINE SHAPE AND ANISOTROPY

It is known that in FMR studies[19] the conductivity may play a key role in determining the absorption line shapes. In insulators the skin depth (δ) is considerably larger than the sample size and the uniform mode is excited in spherical samples. In metals the skin depth is as a rule appreciably smaller than the sample size and the inhomogeneity of the microwave field results in spin-wave excitations. Being magnetic semiconductors, the chromium chalcogenide spinels provide nearly ideal materials to study the effect of the conductivity on the FMR absorption in a very interesting intermediate regime.

The phenomenological description of ferromagnetic resonance implies the study of the set of equations composed by the equation of motion for the time-dependent local magnetization and Maxwell equations, subjected to appropriated boundary conditions.[19] It results that the electromagnetic wave propagates in a medium defined by an effective magnetic permeability containing all information of interest. In particular, the resonance field, $H_{\rm res}$, is defined as the field that maximizes the imaginary (or absorption) part of the effective magnetic permeability.

Neglecting, for the moment, magnetic anisotropy effects, the simplest case is that of an insulating ellipsoidal sample magnetized along the axis of rotation (z axis). In this case one obtains Kittel's condition for uniform resonance:

$$(\omega/\gamma)=[H_{\rm res}-(N_z-N_t)M_s], \tag{1}$$

where ω is the radiation frequency, γ is the spectroscopy ratio, M_s is the saturation magnetization, and $N_t=N_x=N_y$ is the demagnetizing factor in directions perpendicular to the axis of symmetry, satisfying $2N_t+N_z=4\pi$. For a sphere, $N_t=N_z$ and thus $\omega=\gamma H_{\rm res}$.

In a conducting medium,[20] however, the situation gets very complex and the analysis is in general made in distinct regimes according to the material of interest. For a metal such as iron, the radiation penetration (skin) depth, $\delta=c[2\pi\sigma\omega]^{-1/2}$, where c is the light velocity, σ is the conductivity, and ω is the radiation frequency, is quite small. In fact, at room temperature, $\sigma\simeq(2.8)10^4\ \Omega^{-1}\ {\rm cm}^{-1}$, and taking ω=9.4 GHz (our working frequency), we find $\delta\simeq(0.31)10^{-2}$ mm. On the other hand, for a magnetic semiconductor such as $CdCr_2Se_4$ and $HgCr_2Se_4$, σ is at most two orders of magnitude smaller and in turn δ is at least 100 times bigger and thus of the order of the radius of the samples used in our experimental studies. At resonance, estimates for δ may turn substantially smaller due to the enhancement with frequency of the imaginary part of the effective magnetic permeability, which is assumed unity in a classical spin depth derivation. In some cases this enhancement may cause the system to enter in the so-called anomalous skin effect regime,[19] in which case δ is smaller than the electron mean free path.

The main result of the skin effect is that the magnetic excitations associated with the resonance condition are not the uniform mode, as in the case of insulators, but rather spin-wave modes with nonzero values of the wave vector k. Its dispersion relation in an ellipsoidal sample, including exchange and dipolar forces, is given by[19]

$$(\omega_k/\gamma)^2=[(H-N_zM_s+H_{\rm ex}a^2k^2)(H-N_tM_s+H_{\rm ex}a^2k^2+4\pi M_s\sin^2\phi_k)], \tag{2}$$

where $H_{\rm ex}=2A/M_sa^2$ is the exchange effective field, a is the lattice constant, and ϕ_k is the angle between the wave vector $\mathbf{k}$ and the z direction.

In metals the resonance condition is associated to spin-wave excitations with wave vectors that peak at $k\sim\delta^{-1}$. As discussed by Ament and Rado[21] it gives rise to a shift in the resonance field, with respect to the uniform resonance at constant frequency, given by

$$\Delta H_{\rm res}=-\frac{8\pi}{3}\frac{\sqrt{A\sigma\omega}}{c}, \tag{3}$$

and to the so-called exchange-conductivity damping mechanism[19] with a magnitude given by twice the value of $|\Delta H_{\rm res}|$.

On the other hand, in low-conductivity materials, such as ferrites[22] and magnetic semiconductors,[23] the wave vector of the excited spin waves are much smaller, in such a way that the exchange term in Eq. (2) can be neglected in the analysis. In this case, for spherical samples, the resonance condition satisfies[24]

$$(\omega/\gamma)^2=H_i(H_i+4\pi M_s\sin^2\phi_k), \tag{4}$$

$$H_i=H_{\rm res}-(4\pi M_s/3). \tag{5}$$

It results that $\omega_{\rm min}\leqslant\omega\leqslant\omega_{\rm max}$, where $\omega_{\rm min}$ and $\omega_{\rm max}$ correspond to the two limits of the spin-wave manifold, $\phi_k=0$ and $\phi_k=\pi/2$, respectively, and manifest as maxima in the density of states of a continuum of modes between these angle limits. Notice that, at constant frequency, $H_{\rm res}(\phi_k=\pi/2)$ is shifted towards low fields and $H_{\rm res}(\phi_k=0)$ towards the high-field side. In the case of ferrites, a quite detailed study in this regime of validity was carried out by Saito, Marysko, and collaborators.[22,24] In the following we shall argue that their approach applies also to the case of chromium chalcogenide spinels for samples with sufficiently high conductivity.

Figure 1 shows the FMR line shapes of a spherical sample of $CdCr_2Se_4$ doped with Ag at 5.4 mole %, Φ=0.54 mm at several temperatures. At low temperatures the line is symmetrical about the field of resonance, characterizing the excitation of the uniform mode. As the temperature increases,

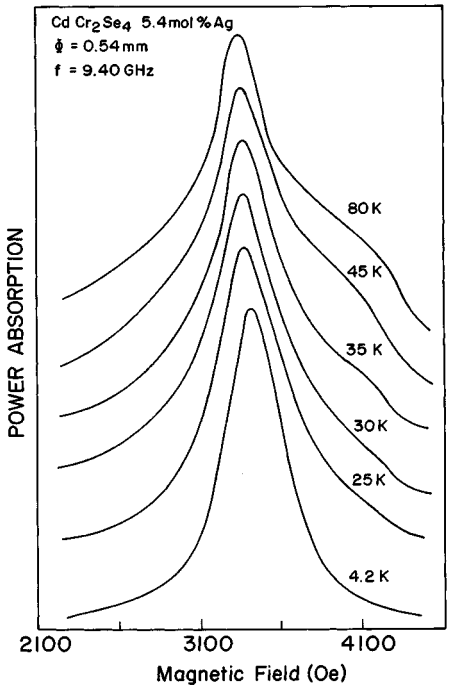

FIG. 1. Temperature variation of the FMR line shape along the [110] direction for 5.4 mole % Ag-doped $CdCr_2Se_4$, $\Phi=0.54$ mm at 9.40 GHz.

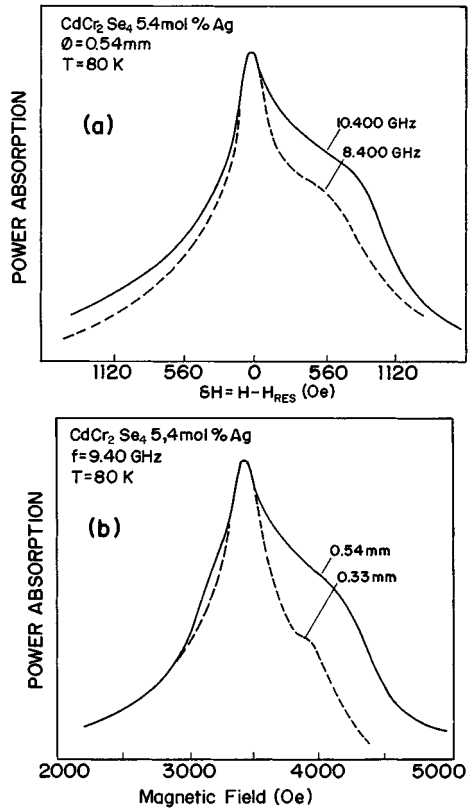

FIG. 2. Variation of the FMR line shape: (a) with the frequency and (b) with the diameter for spherical samples of 5.4 mole % Ag-doped $CdCr_2Se_4$ at 80 K.

the line becomes asymmetrical with a terrace edge (or a shoulder) on the high-field side of the main absorption maximum. This behavior contrasts with those observed in samples with lower Ag doping, for which the line shapes are symmetrical throughout the whole temperature range, but agrees with the line-shape profile observed in ferrites. The peak at low (high) fields corresponds to the excitation of spin waves with wave vector perpendicular (parallel) to the direction of the applied magnetic field. Notice that the $H_{\rm res}(\phi_k=\pi/2)$ peak shifts towards low fields with increasing temperature as a result of the increase in the sample conductivity, consistently confirmed in the next section. The exchange-conductivity mechanism, Eq. (3), usually produces exactly the opposite temperature dependence, as observed in metals,[20] due to the increase of $\sigma(T)$ with decreasing temperature.

In Fig. 2 we display the frequency and size dependences[16] of the absorption. As the frequency increases, the skin depth decreases and the peak near $H_{\rm res}(0)$ becomes more pronounced. The separation between the shoulder and the main absorption peak for the 0.33 mm diam sample of $CdCr_2Se_4$ with 5.4 mole % of Ag is 800 Oe. This is appreciably smaller than the theoretical value of 1300 Oe, estimated from[22]

$$\delta H=\frac{\omega}{\gamma}+2\pi M_s-\left[(2\pi M_s)^2+\left(\frac{\omega}{\gamma}\right)^2\right]^{1/2}, \tag{6}$$

where $4\pi M$ (80 K)=3540 Oe. However, when the sample diameter increases to 0.54 mm, the separation increases to 1000 Oe, approaching the theoretical value, as expected, since the sample dimension becomes larger than the skin depth. We thus conclude that this is indeed the case of spin-wave excitation in a region in which exchange effects can be neglected. Our studies in the next section will also confirm this conclusion.

We now turn to study the effect of magnetic anisotropy on the FMR properties. The dependence of the resonance condition on crystal orientation can be introduced[19] via an internal effective anisotropy field, $\mathbf{H}_i^{(a)}$, derived from the volume anisotropy energy density, defined by

$$\mathbf{H}_i^{(a)}=\delta F_{(a)}(\alpha_j)/\delta\mathbf{M}, \tag{7}$$

$$F_{(a)}(\alpha_j)=K_1S+K_2P+K_3S^2, \tag{8}$$

where $\mathbf{M}$ is the magnetization, α_j, $j=1$, 2, and 3, are the direction cosines of the magnetization with respect to the [100], [010], and [001] axes of the crystal, respectively, $S=\alpha_1^2\alpha_2^2+\alpha_2^2\alpha_3^2+\alpha_1^2\alpha_3^2$ and $P=\alpha_1^2\alpha_2^2\alpha_3^2$. The field (7) may now be included in the resonance condition through the effective anisotropic demagnetizing factor defined by

$$\mathbf{H}_i^{(a)}=-\mathbf{N}^{(a)}\cdot\mathbf{M}. \tag{9}$$

One can show that the general expressions for the three principal anisotropy constants, $N_x^{(a)}$, $N_y^{(a)}$, and $N_z^{(a)}$ are [the static and rf magnetic fields lay in the (110) plane of a cubic crystal]

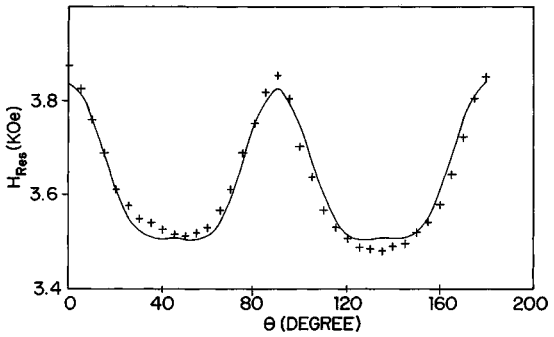

FIG. 3. Angular dependence of $H_{\rm res}$ for 1.3 mole% Ag-doped $HgCr_2Se_4$, $\Phi=0.71$ mm at 9.4 GHz and 15 K. θ is the angle between the static magnetic field and the [100] direction in the (110) plane. The curve is a fitting of Eq. (12a) using the parameters values in Oe: $\beta_0=3836.8$; $(K_1/M)=-726.9$; $(K_2/M)=-2863.1$; $(K_3/M)=1428.94$.

$$N_x^{(a)}=\frac{K_1}{M_s^2}(2-3\sin^2\theta)-\frac{K_2}{M_s^2}\sin^2\theta\cos^2\theta+\frac{K_3}{K_s^2}\left(4\sin^2\theta-9\sin^4\theta+\frac{9}{2}\sin^6\theta\right), \tag{10a}$$

$$N_y^{(a)}=\frac{K_1}{M_s^2}(2-9\sin^2\theta+9\sin^4\theta)+\frac{K_2}{M_s^2}\left(3\sin^2\theta-10\sin^4\theta+\frac{15}{2}\sin^6\theta\right)+\frac{K_3}{M_s^2}\left(12\sin^2\theta-53\sin^2\theta+\frac{147}{2}\sin^6\theta-\frac{63}{8}\sin^8\theta\right), \tag{10b}$$

$$N_z^{(a)}=\frac{K_1}{M_s^2}(4\sin^2\theta-3\sin^4\theta)+\frac{K_2}{M_s^2}\left(\frac{3}{2}\sin^4\theta-\frac{3}{2}\sin^6\theta\right)+\frac{K_3}{M_s^2}\left(8\sin^4\theta-12\sin^6\theta+\frac{9}{2}\sin^9\theta\right). \tag{10c}$$

In deriving Eqs. (10) it is assumed that the crystal is magnetized to saturation and both the magnetization and the magnetic field are along the z direction, which makes an angle θ with the [001] crystal axis.

We may now introduce anisotropy effects on the resonance condition, Eq. (4), by modifying the static internal magnetic field in the form

$$H_i=H_{\rm res}-\frac{4\pi}{3}M_s-\frac{K_1}{M_s}(4\sin^2\theta-3\sin^4\theta)-\frac{K_2}{M_s}\left(\frac{3}{2}\sin^4\theta-\frac{3}{2}\sin^6\theta\right)-\frac{K_3}{M_s}\left(8\sin^4\theta-12\sin^6\theta+\frac{9}{2}\sin^8\theta\right). \tag{11}$$

By putting $\phi_k=\pi/2$, substituting (11) into (4,5), and solving for the field of maximum absorption in the (110) plane, we obtain

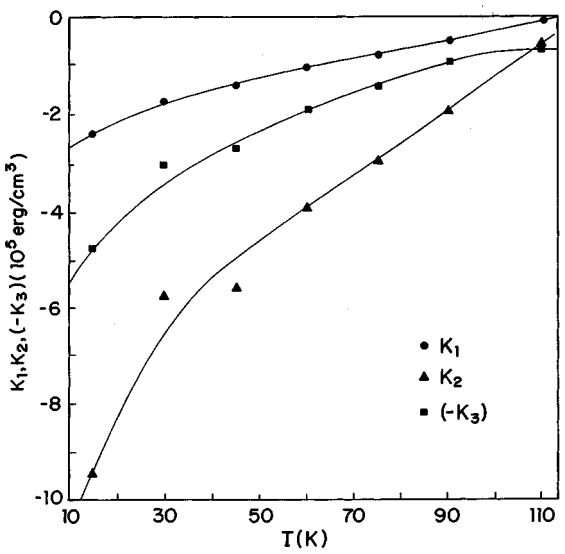

FIG. 4. Temperature dependence of the anisotropy constants: K_1 (●), K_2 (▲), and K_3 (■) for 1.3 mole% Ag-doped $HgCr_2Se_4$. The lines are guides for the eyes.

$$H_{\rm res}(\theta)=\beta_0+\frac{K_1}{M_s}\left(\sin^2\theta+\frac{3}{2}\sin^2 2\theta\right)+\frac{K_2}{M_s}\left(\frac{3}{2}\sin^4\theta-\frac{3}{2}\sin^6\theta\right)+\frac{K_3}{M_s}\left(8\sin^4\theta-12\sin^6\theta+\frac{9}{2}\sin^8\theta\right), \tag{12a}$$

where

$$\beta_0=\sqrt{\omega^2/\gamma^2+4\pi^2M_s^2}-\tfrac{2}{3}\pi M_s. \tag{12b}$$

Using Eqs. (12) we can estimate the first three anisotropy constants from the data for $H_{\rm res}(\theta)$ by curve fitting with a least-squares method.

Figure 3 shows a typical fitting using Eq. (12a) of the data for $H_{\rm res}(\theta)$ from a sphere ($\Phi=0.71$ mm) of 1.3 mole% Ag-doped $HgCr_2Se_4$ at 15 K and 9.4 GHz. Similar fittings give values for K_1, K_2, and K_3 as a function of temperature, as shown in Fig. 4. Attempts at fitting the data using Kittel's condition for uniform resonance, Eq. (1), have failed for this sample with relatively high conductivity.

III. FMR LINEWIDTH

If the skin depth is larger than or of the order of the sample size, the temperature dependence of the linewidth (ΔH) of a magnetic semiconductor can be explained by various relaxation mechanisms,[12,25] such as two-magnon scattering due to surface and volume pits, eddy-current losses, and slow or fast impurity relaxations. In Fig. 5 we show the results of the temperature dependence of ΔH for three samples of Ag-doped $CdCr_2Se_4$ single crystals with 0.1% ($\Phi=0.5$ mm), 0.75% ($1.0\times0.6\times0.2$ mm^3), and 5.4% ($\Phi=0.5$ mm) nominal doping. As we see from this figure, above 80 K ΔH varies little with temperature until one reaches the critical region. We interpret the rapid increase of ΔH in this region as due to the large magnetic fluctuations.

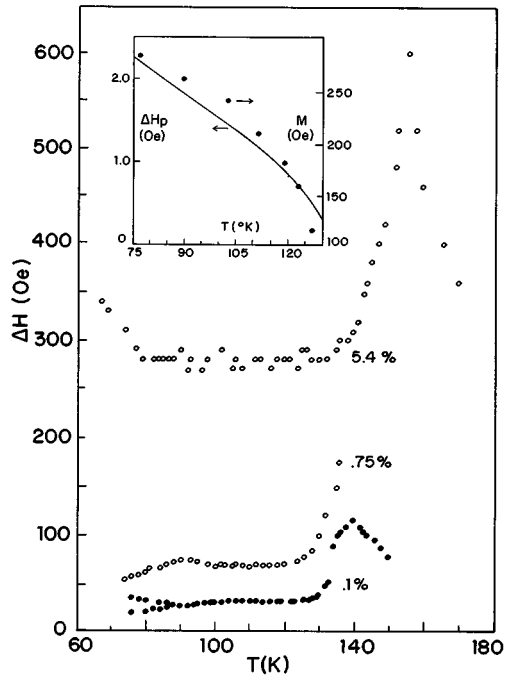

FIG. 5. FMR linewidth of Ag-doped $CdCr_2Se_4$ single crystals as a function of temperature. The inset shows data for the magnetization (from Ref. 26) and our theoretical prediction (interpolation of dot points) of the temperature dependence of the linewidth due to pit scattering for undoped $CdCr_2Se_4$.

For the sample with 5.4% Ag one may conclude that T_C increased about 10 K as a resulting of doping. Below 85 K we can notice, for a sample with 0.1% Ag, a splitting of ΔH corresponding to two different crystallographic directions. In fact, an anomalous increase of ΔH along the [100] direction was detected by Bairamov *et al.*[10] (no effect was felt along the [111] direction), below liquid nitrogen, and has been attributed to the presence of impurity Cr^{4+} ions. This effect is also seen in the ΔH of sample with 5.4% Ag for $T<80$ K. The ΔH of a sample with 0.75% Ag does not show it because the sample was oriented in the [111] direction (a maximum around 90 K might be due to some impurity effect). As will become clear in this and the next sections, the above-mentioned anomalies in ΔH are due to the presence of Cr^{2+} and/or Cr^{4+} ions, whose valences have been changed to charge compensate for modifications in the sample stoichiometry. They are strongly dependent on the crystallographic directions, as opposed to the quite isotropic exchange-conductivity mechanism discussed in the last section.

The contributions of intrinsic processes involving thermal magnons and phonons are of the order 0.1–1 Oe and therefore may be neglected in our discussion. To estimate the losses due to two-magnon scattering we shall consider the treatment of Sparks[26] for surface and volume pits. In the absence of information about the volume of the pits let us assume a total contribution of 5 Oe at $T=4.2$ K (the 0.5 μm surface pits gives a contribution of 2.74 Oe and the difference is to account for the volume ones), which is of the order of magnitude found for ΔH in undoped $CdCr_2Se_4$ single crystal.[27] The temperature dependence of both mechanisms is the same and determined by the magnetization[26] (see inset in Fig. 6). For the indirect processes we shall consider the

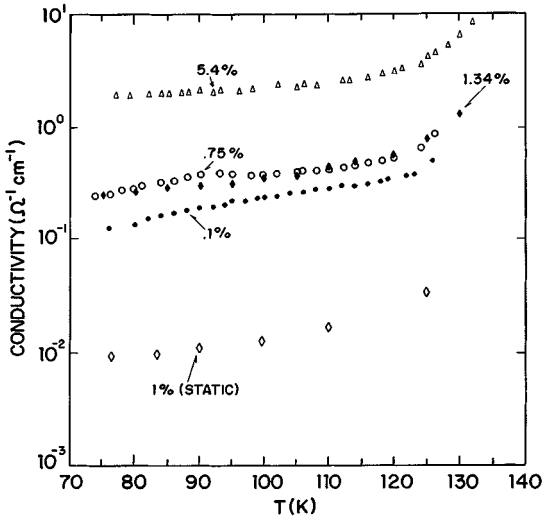

FIG. 6. Microwave conductivities of Ag-doped $CdCr_2Se_4$ single crystals as a function of temperature using Eq. (18). Nominal doping: (△) 5.4%; (◆) 1.34% (ΔH data from Ref. 10); (○) 0.75%; (●) 0.1% (bottom data for ΔH in Fig. 5), at 9.4 GHz; and (◇) indicates data (Ref. 28) of the static conductivity for 1% Ag.

eddy-current losses in spherical samples as given by[25]

$$\Delta H=\frac{16\pi R^2\omega}{45c^2}4\pi M\sigma_\omega, \tag{13}$$

where R is the radius of the sample, ω is the microwave frequency, M is the magnetization, and σ_ω is the crystal conductivity at frequency ω. For samples in the form of a slab, the eddy-current losses are written in the form[25]

$$\Delta H=\frac{8\pi d^2\omega}{c^2}4\pi M\sigma_\omega, \tag{14}$$

where d is the dimension of the slab in the wave-vector direction. Thus the temperature dependences of the microwave conductivity to fit the data are obtained from the equation

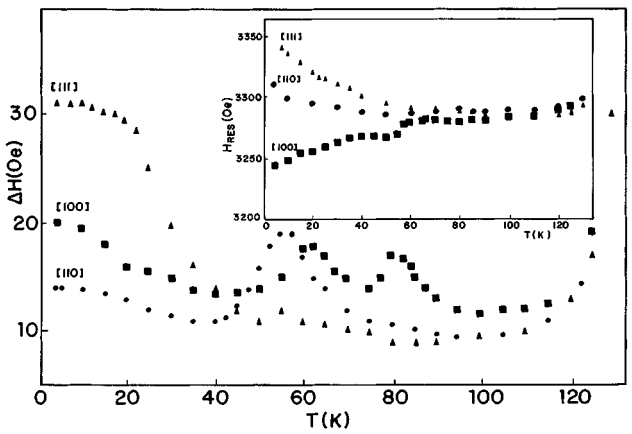

FIG. 7. Temperature dependence of ΔH for 0.1 mole% Ag-doped $CdCr_2Se_4$, $\Phi=0.30$ mm at 9.4 GHz. The inset shows the temperature dependence of H_{res} for the same sample.

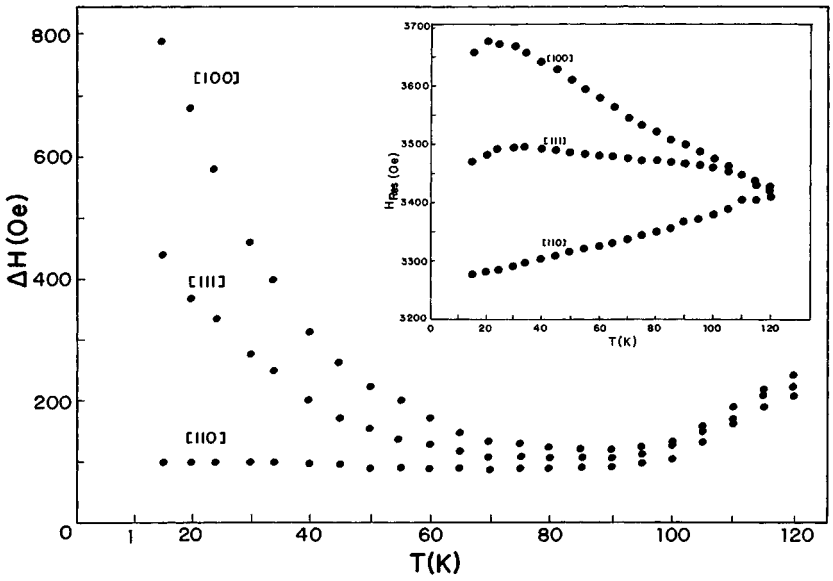

FIG. 8. Temperature dependence of ΔH along the principal crystalographic directions in a sample of ''as grown'' $HgCr_2Se_4$, $\Phi=0.8$ mm at 9.4 GHz. The inset shows the temperature dependence of $H_{\rm res}$.

$$\sigma_\omega(T)=\frac{\Delta H(T)-\Delta H_p(T)}{AM(T)}, \tag{15}$$

where $\Delta H(T)$ is the experimental value, $\Delta H_p(T)$ is the pit-scattering contribution, and A is found from (13) or (14).

In Fig. 6 we present the results for $\sigma_\omega(T)$ using (15), and for comparison we also show the $\sigma_\omega(T)$ to fit the data of Bairamov *et al.*[10] (along the [111] direction) for a spherical sample of 1.34% Ag-doped $CdCr_2Se_4$, $\Phi=0.3$ mm, as well as the temperature dependence of the static conductivity for 1% Ag-doped $CdCr_2Se_4$.[28] These values would change very little if we had assumed a ΔH_p of 10 Oe. The calculated microwave conductivities are about one order (0.1, 0.75, and 1.34%) and are two orders (5.4%) of magnitude greater than the static one (1%) but the temperature dependences are quite the same. The conductivities for 0.75 and 1.34% are practically the same, which may be due to uncertainties associated with the nominal doping. This increase with frequency should be expected by taking into account the impurity contribution to the conductivity and was in fact found for *n*-type $CdCr_2Se_4$ (Ref. 29) and EuO.[30]

In Fig. 7 we shown the results of the temperature dependences of $H_{\rm res}$ and of ΔH for a sample of 0.1 mole% Ag-doped $CdCr_2Se_4$ single crystal. As shown in this figure, $H_{\rm res}$ and ΔH present maxima for various directions at various temperatures. These features will be discussed in Sec. VI.

In Fig. 8 we show the results of the temperature dependences of $H_{\rm res}$ and ΔH for a spherical sample of ''as grown'' $HgCr_2Se_4$ single crystal, $\Phi=0.8$ mm. Below 70 K we can notice anomalous increase of ΔH along the [100] and [111] directions. To explain the giant anomalous peaks of $H_{\rm res}$ and ΔH along some particular crystallographic directions, we assume that the impurity ion has two low-lying energy levels so that these anomalies would occur at crossover or near crossover of these levels. The ground state would result from a combined effect of crystalline field, spin-orbit coupling, and exchange interaction between the magnetic moment of the impurity ion and the crystal magnetization.

Our analysis shows that two different mechanisms can fit the temperature dependence of ΔH at low temperatures: the fast (or transverse) or the slow (or longitudinal) relaxation mechanism.[26] The slow or longitudinal relaxation mechanism is induced by the delay in establishing the thermal equilibrium values of the population of the impurity ion energy. These levels are modulated by the uniform precession via an anisotropic exchange coupling between the spin of the impurity ion and the crystal magnetization. For the two-level system the expression for the FMR linewidth reads[26]

$$\Delta H=\frac{N_{\rm imp}}{kTM_s}f(\theta,\phi)\frac{\omega\tau}{1+(\omega\tau)^2}\mathrm{sech}^2\left(\frac{\Delta\epsilon}{2kT}\right), \tag{16}$$

where

$$f(\theta,\phi)=\frac{1}{4}\left[\left(\frac{\partial\Delta\epsilon}{\partial\theta}\right)^2+\left(\frac{\partial\Delta\epsilon}{\partial\phi}\right)^2\right]. \tag{17}$$

Here ω is the resonance frequency, $N_{\rm imp}$ is the density of impurity ions, $\Delta\epsilon$ is the separation between the energy levels, M_s is the saturation magnetization, θ and ϕ are the angular coordinates of the magnetization with respect to the equilibrium position, k is the Boltzmann constant, and τ is the relaxation time associated with restoring thermodynamic equilibrium in the population of the two energy levels. It is worth noticing that ΔH in Eq. (16) may have two maxima as a function of T.

The temperature dependence of τ is determined by the thermal bath which we assume to consist of phonons or magnons. For direct processes in which a phonon (or magnon) is absorbed or emitted, the relaxation time has the same temperature dependence, namely

$$\tau=\tau_0\tanh\left(\frac{\Delta\epsilon}{2kT}\right). \tag{18}$$

In the transverse or fast relaxation mechanism, the transverse part of the effective field acting on the impurity ion excites the precession of it, as in a paramagnetic resonance experiment, and energy is transferred from the ferromagnetic system to the thermal bath. In the case of two energy levels, and $h\omega\ll\Delta\epsilon$, the expression for the FMR linewidth corresponding to this process is given by[26]

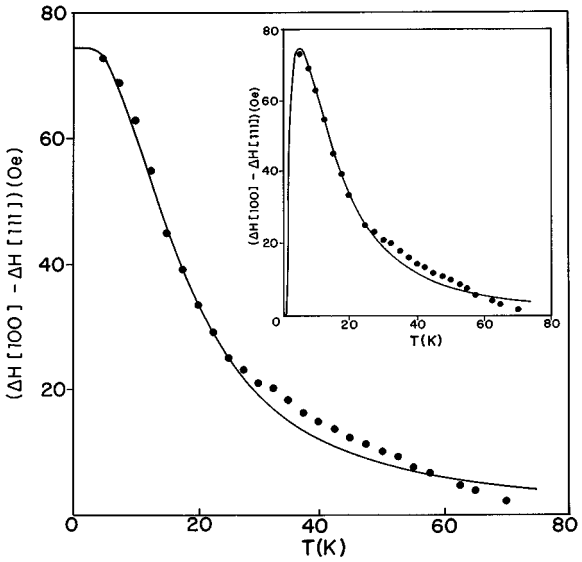

FIG. 9. Temperature dependence of ΔH data (from Ref. 10) for 1.3 mole% Ag-doped $CdCr_2Se_4$. The curve is our fitting assuming the fast relaxation mechanisms as in Eqs. (16)–(18): $\tau_0=3.3\times10^{-13}$ s and $\Delta\epsilon=\Delta E_x=16.7$ cm^{-1}. The inset shows our fitting now assuming the slow relaxation mechanism as in Eqs. (18) and (19): $\tau_0=1.4\times10^{-10}$ s and $\Delta\epsilon=2.46$ cm^{-1}.

$$\Delta H=4\frac{N_{\rm imp}}{N_0}\frac{\omega}{\gamma}\frac{(\Delta\epsilon\tau/\hbar)}{[1+(\Delta\epsilon\tau/\hbar)^2]}\tanh\frac{\Delta\epsilon}{2kT}, \qquad (19)$$

where N_0 is the density of Cr^{3+} ions forming the magnetically ordered subsystem. We should notice that ΔH in Eq. (19) has a maximum at $T=0$ and decreases with increasing temperature.

In Fig. 9 we present our fit of the ΔH peak for the data of 1.34 mole% Ag-doped $CdCr_2Se_4$, from Ref. 10, using the mentioned mechanisms. We have subtracted the results of ΔH for the [100] direction from the ones for the [111] direction to isolate the contribution from the impurity ions. To produce the fit of Fig. 9 the following values for $\Delta\epsilon$ and τ_0 were obtained: $\Delta\epsilon=16.7$ cm^{-1} and $\tau_0=3.3\times10^{-13}$ s, and $\Delta\epsilon=2.46$ cm^{-1} and $\tau_0=1.4\times10^{-10}$ s, for the fast and the slow mechanisms (inset), respectively. We have used $M_s=4480$ Oe and $\omega=6.28\times10^{10}$ s^{-1}. On the other hand, in Fig. 10 we show that only a slow relaxation mechanism can fit our data of Fig. 8 for ''as grown'' $HgCr_2Se_4$ (subtracting now the data for the [110] direction) with $\tau_0=1.8\times10^{-11}$ s and $\Delta\epsilon=16$ cm^{-1} for the [100] direction. In the inset it is also shown that the same parameters can nicely fit the data of Ref. 10 for a similar sample of ''as grown'' $HgCr_2Se_4$. The fitting for the [111] direction will be discussed in Sec. VI.

In the next section the energy levels of the Cr ions in their proper crystal environment will be calculated allowing a microscopic interpretation of the magnetic anisotropy and linewidth data presented in Secs. II and III.

IV. LEVEL STRUCTURES OF Cr IONS IN CHALCOGENIDE SPINELS

The chromium chalcogenides[1] have a normal spinel structure (see Fig. 11). The Cr ions (B sites) are surrounded by an octahaedron of selenium ions. Each B site lies on an axis of

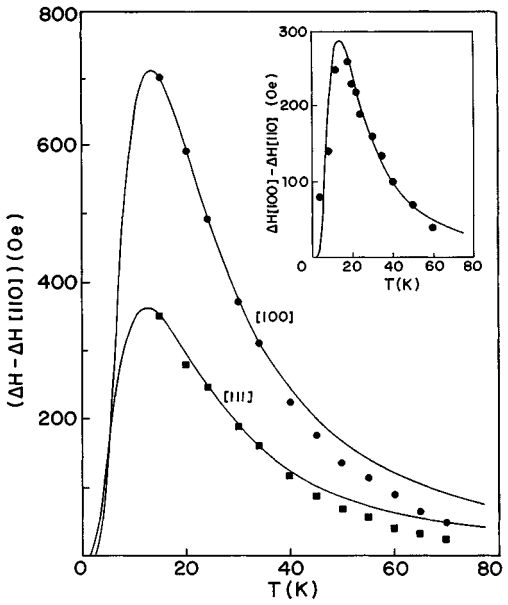

FIG. 10. Temperature dependence of ΔH for ''as grown'' $HgCr_2Se_4$, $\Phi=0.80$ mm at 9.4 GHz. The curves are fittings of the slow relaxation mechanism [using Eqs. (25) and assuming a statistical distribution over the distinct B sites]: $\tau_0=1.8\times10^{-11}$ s and $\Delta\epsilon=\Delta E_x=16.0$ cm^{-1} for the [100] direction and $\tau_0=1.8\times10^{-11}$ s, $\Delta E_x=16.0$ cm^{-1}, and $D=9.0$ cm^{-1} for the [111] direction.

threefold symmetry which is parallel to one of the body diagonals of the cubic crystal. The local symmetry about a B site is not cubic but trigonal. Four kinds of B sites may be distinguished according to which one of the four directions [111], [$\bar{1}$11], [1$\bar{1}$1], and [11$\bar{1}$] is parallel to the trigonal axis. The selenium positions are displaced slightly from those of a regular octahedron. Two contributions to the trigonal field may be distinguished. The cations (Cd ions occupying tetrahedral positions, or A sites) tend to make the potential greatest along the trigonal axis. The anions (Se ions) oppose the effect of the cations.[31]

Since $kT_C\cong90$ cm^{-1}, to calculate the temperature dependence of the anisotropy we need the energy levels within this

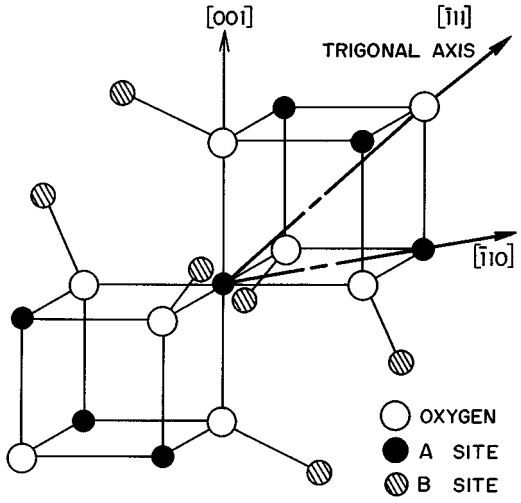

FIG. 11. Spinel structure showing the immediate environment of an octahedral site.

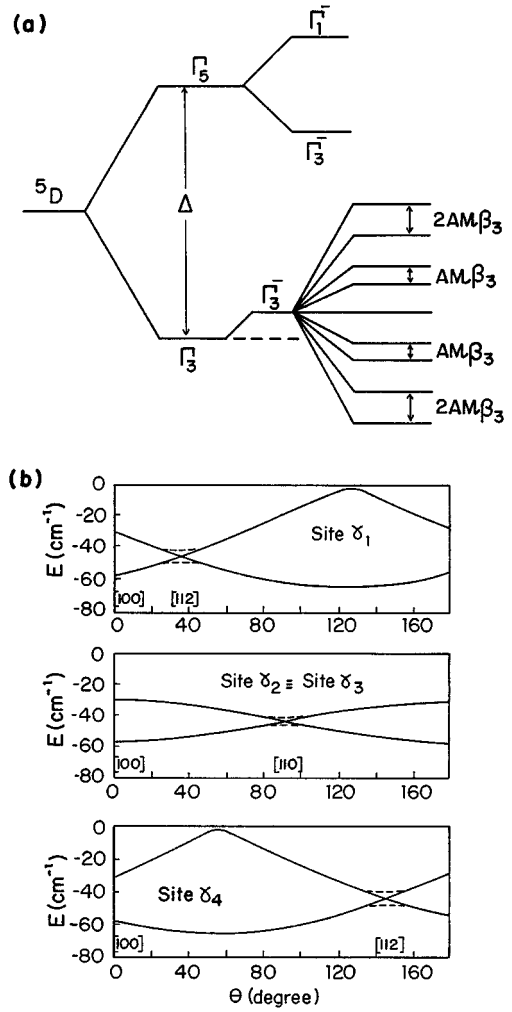

FIG. 12. Energy levels of the Cr^{2+} ions in chromium chalcogenide spinels. (a) Energy levels scheme for $3d^4$ configuration on an octahedral site. (b) Angular dependence of the low-lying energy levels. The parameters used are $A=23.0$ cm^{-1}, $\eta=0.996$ ($\lambda=55.0$ cm^{-1} and $\Delta E_x=16.7$ cm^{-1}). Level crossing occurs along the [112] direction at site γ_1, along the [110] direction at sites γ_2 and γ_3, and along the [112] direction at site γ_4. The dotted lines illustrate the level splitting obtained in higher order of perturbation theory.

range, i.e., the level structure of the orbital ground state. Starting from the $(2L+1)(2S+1)$ fold-degenerate state, we consider medium crystal field and use the perturbative method of Bleaney and Stevens.[32]

A. Cr^{2+} in octahedral sites ($3d^4$-^5D state, $L=2$, $S=2$)

The cubic crystal field splits the ^5D state into a Γ_5 triplet and a Γ_3 doublet orbital ground state. The trigonal field does not remove the orbital degeneracy, and its effect is calculated to first order in perturbation theory. We have now to include the spin-orbit interaction and the action of the molecular field of the Cr^{3+} host ions on the spin of the Cr^{2+} impurity ion, both to first order. For symplicity, we shall neglect the Zeeman and the dipolar spin-spin interactions. The tenfold Γ_3^- orbital-spin-multiplet finally splits [see Fig. 12(a)] with eigenvalues,

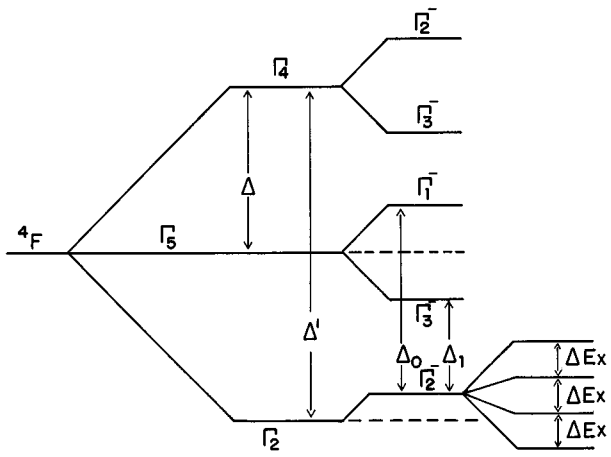

FIG. 13. Energy levels of the Cr^{3+} ions in chromium chalcogenide spinels ($3d^3$ configuration on an octahedral site).

$$E_{\alpha,i}=0 \quad \text{(doublet)}, \tag{20a}$$

$$E_{\alpha,i}=\pm\sqrt{(\tfrac{5}{2}\pm\tfrac{3}{2})}\sqrt{(1\pm\eta\beta_{3i})}, \tag{20b}$$

$$A=\sqrt{(\Delta E_x)^2+8(\lambda v/\Delta)^2}, \tag{20c}$$

$$\eta=\frac{4\sqrt{2}\Delta v\lambda\Delta E_x}{\Delta^2(\Delta E_x)^2+8\lambda^2 v^2}, \quad |\eta|<1, \tag{20d}$$

where α runs over the tenfold level structure and i over the four distinct B sites, ΔE_x is the exchange energy between the Cr^{2+} ions and the host Cr^{3+} ions, λ is the spin-orbit coupling, Δ is the cubic crystal-field splitting, v is the trigonal component resulting from the off-diagonal component of the crystal field within the orbital doublet Γ_3, and β_{3i} is the direction cosine of the magnetization with respect to the coordinate system in which the z axis is along one of the four [111] directions (local axis of deformation), as shown in Fig. 12(b). It should be mentioned that in calculating the energy eigenvalues, the angular momentum was quantized along the local axis of deformation and the spin along the direction of magnetization.

Our results for the level structure of the Cr^{2+} ions differ from those obtained by Hoekstra and van Stapele.[8] In the latter the orbital ground state splits by the combined action of spin-orbit coupling and trigonal field in second-order perturbation theory, whereas the exchange (molecular) field is taken to be infinite. Contrary to the latter assumption, we take the molecular field of the order of the spin-orbit coupling and their effect is calculated in first order using wave functions including first-order corrections from the trigonal field. Comparison with experimental data in Sec. VI indicates that our viewpoint is more adequate to describe the anisotropy of $CdCr_2Se_4$.

B. Cr^{3+} in octahedral sites ($3d^3$-^4F state, $L=3$, $S=3/2$)

The cubic crystal field splits the ^4F state into a Γ_2 singlet and two Γ_4 and Γ_5 triplets (see Fig. 13). For this ion on a octahedral site of a spinel structure, the ground state is an orbital singlet (Γ_2) and the exchange (molecular field), spin-orbit, and spin-spin splittings are small compared to the

spacing of the excited levels in the crystal field. Thus the orbital angular momentum is quenched to first-order perturbation theory and the one-ion energy spectrum can be obtained from a spin Hamiltonian in the form[33]

$$H_s + CS_{z'} + DS_z^2, \tag{21}$$

with

$$C \cong \Delta E_x,$$
$$D \cong 6\sqrt{5}\frac{\lambda^2 v}{\Delta^2} - \rho\left[5 - 2\sqrt{5}\frac{v}{\Delta}\right], \tag{22}$$

where Δ is the cubic-field splitting, v is the trigonal component resulting from off-diagonal elements of the crystal field between the orbital singlet Γ_2 and the orbital triplet Γ_5, ρ is the constant of the dipolar spin-spin interaction, z' is the axis along the magnetization direction, and z is the axis along one of the four directions [111].

Assuming $|D| \ll |C|$, and perturbation theory to the third order, we obtain the following lowest-energy levels (see Fig. 13) for the Γ_2^- spin multiplet:

$$E_{\pm 3/2} = \pm\frac{3}{2}\Delta E_x + \frac{3}{4}D \pm \frac{3D^2}{8\Delta E_x} - \frac{9D^3}{64\Delta E_x^2} + \left(\frac{3D}{2} \pm \frac{9D^2}{4\Delta E_x} - \frac{9D^3}{4\Delta E_x^2}\right)\beta_{3i}^2 + \left(\pm\frac{21D^2}{8\Delta E_x} - \frac{117D^3}{64\Delta E_x^2}\right)\beta_{3i}^4 + \frac{135D^3}{32\Delta E_x^2}\beta_{3i}^6, \tag{23a}$$

$$E_{\pm 1/2} = \pm\frac{\Delta E_x}{2} + \frac{7D}{4} \pm \frac{3D^2}{8\Delta E_x} - \frac{21D^3}{64\Delta E_x^2} + \left(\frac{3D}{2} \pm \frac{15D^2}{4\Delta E_x} - \frac{69D^3}{16\Delta E_x^2}\right)\beta_{3i}^2 + \left(\pm\frac{27D^2}{8\Delta E_x} + \frac{567D^3}{64\Delta E_x^2}\right)\beta_{3i}^4 - \frac{135D^3}{32\Delta E_x^2}\beta_{3i}^6. \tag{23b}$$

C. Cr^4 in octahedral sites ($3d^2$-^3F state, $L=3$, $S=1$)

The cubic crystal field splits the ^3F state into two Γ_4 and Γ_5 triplets and one Γ_2 singlet which are further splitted by the trigonal field. The lower state Γ_4 is split into a Γ_2^- singlet and a Γ_3^- doublet. In the selenide compounds there is neither experimental nor theoretical evidence about the sign of the trigonal splitting, Δ_T. Thus the lowest state may be either the Γ_3^- state ($\Delta_T > 0$) or the Γ_2^- state ($\Delta_T < 0$) [see Fig. 14(a)]. Both cases are considered in this section. To calculate the energy levels we have now to include the spin-orbit interaction and the action of the molecular field of the Cr^{3+} host ions on the spin of the Cr^{4+} impurity ion. For simplicity, we shall also neglect the Zeeman and the dipolar spin-spin interactions.

1. Γ_3^- lowest

The effect of the above-mentioned interactions (to first order) on the Γ_3^- spin multiplet splits this state, with the new eigenvalues

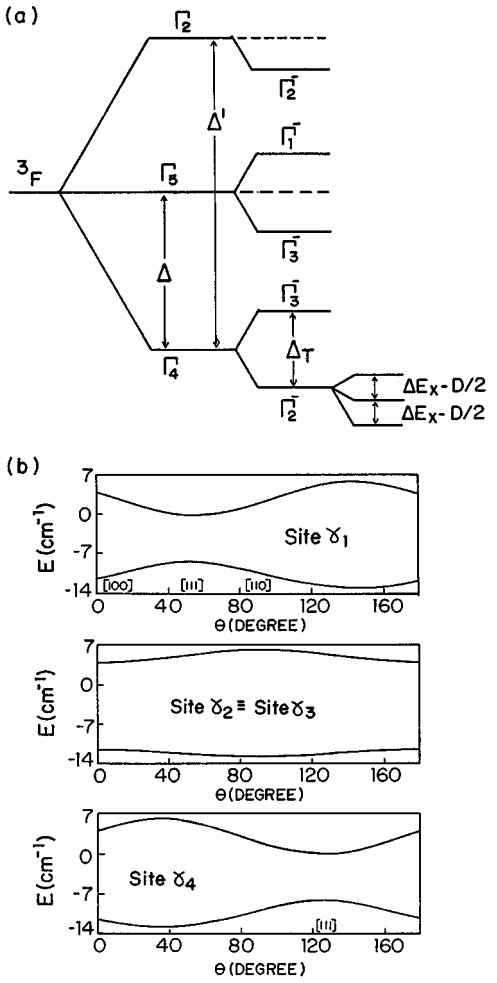

FIG. 14. Energy levels of the Cr^{4+} ions in chromium chalcogenide spinels. (a) Energy levels scheme for $3d^{2+}$ configuration on an octahedral site. (b) Angular dependence of the low-lying energy levels. The parameters used are $\Delta E_x = 16.0\ \mathrm{cm}^{-1}$ and $D = 9.0\ \mathrm{cm}^{-1}$.

$$E_{\alpha,i} = 0 \quad \text{(doublet)}, \tag{24a}$$

$$E_{\alpha,i} = \pm\lambda x(1 + \gamma^2 \pm \gamma\beta_{3i})^{1/2}, \tag{24b}$$

where α now runs over the sixfold level structure, $\gamma = \Delta E_x/\lambda x$, $x = 3/2 + \sqrt{5}(v/\Delta)$, and v is the trigonal component resulting from off-diagonal elements of the crystal field within the orbital triplet Γ_4.

2. Γ_2^- lowest

Being a singlet-orbital ground state, its analysis is quite similar to that of the Cr^{3+} ion, where a spin Hamiltonian, Eq. (21), is derived.

Assuming $|\lambda| \simeq |\Delta E_x|$, and both smaller than the spacing of the excited energy levels, we can consider their effect in perturbation theory. To first order the spin-orbit interaction does not remove the degeneracy of the Γ_2^- state, which is split by the exchange field into three levels separated by ΔE_x. In second order, we find the following eigenvalues for the Γ_2^- spin multiplet (see Fig. 13):

$$E_{1,i} = -\Delta E_x - \frac{D}{2}(3 - \beta_{3i}^2), \tag{25a}$$

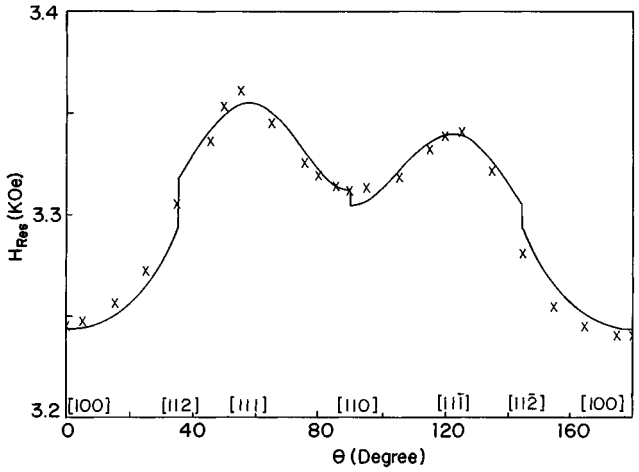

FIG. 15. Angular dependence of $H_{\rm res}(\theta)$ for $CdCr_2Se_4$ with 0.1 mole% Ag, $\Phi=0.30$ mm at 9.4 GHz and 4.2 K. θ is the angle between the static magnetic field and the [100] direction in the (110) plane. The curve is a fitting including additional noncubic anisotropy components due to Cr^{2+} impurity ions (values in Oe): $(\omega/\gamma)=32998.5$; $(K_M/M_s)=-6.2$; $(K_F/M_s)=-3.8$; $(K_1/M_s)=4.1$; $(K_2/M_s)=71.4$.

$$E_{0,i}=-D(1+\beta_{3i}^2), \tag{25b}$$

$$E_{-1,i}=\Delta E_x-\frac{D}{2}(3-\beta_{3i}^2), \tag{25c}$$

with

$$D=\left(9+6\sqrt{5}\frac{v}{\Delta}\right)\frac{\lambda^2}{4\Delta_T}. \tag{26}$$

V. CHROMIUM SINGLE-ION ANISOTROPY IN CHALCOGENIDE SPINELS

In order to calculate the anisotropy due to the chromium ions let us determine their contribution to the free energy per unit volume:

$$F(T=0\ \ \mathrm{K})=\frac{N}{4}\sum_{i=1}^{4}E_{0,i}, \tag{27}$$

$$F(T)=-\frac{NkT}{4}\sum_{i=1}^{4}\ln Z_i, \tag{28}$$

$$Z_i=\sum_{\alpha}\exp\left(\frac{-E_{\alpha,i}}{kT}\right), \tag{29}$$

where $E_{0,i}$ is the ground-state energy, $E_{\alpha,i}$ is the αth energy level for a ion on an octahedral site i, N is the number of impurity chromium ions per cm^3, and a statistical distribution over the distinct B sites is assumed.

A. Cr^{2+} anisotropy

It is clear that Eq. (20b) implies level crossing of the two low-lying energy levels according to the sign of β_{3i} [see Fig. 12(b)]. Using values for A and $\eta(<0)$ which fit our data, this effect is illustrated in Fig. 15, where β_{3i} is related to the cosine directions α_j of the magnetization with respect to the [100], [010], and [001] axes of the crystal. For an applied magnetic field in the (110) plane, we define θ as the angle between the direction of magnetization and the [100] crystal axis ($\theta=0$). Level crossing occurs along the [112] direction [$\theta=\tan^{-1}(1/\sqrt{2})$] at site γ_1, along the [$\underline{1}10$] direction ($\theta=\pi/2$) at sites γ_2 and γ_3, and along the [112] direction at site γ_4.

Using the ground-state energy in the form [see Eq. 20(b)]

$$E_{0,i}=-2A(1-\eta|\beta_{3i}|)^{1/2}, \tag{30}$$

we obtain the following zero-temperature free-energy expressions, according to the θ interval: $0<\theta<\tan^{-1}1/\sqrt{2}$:

$$F_1(T=0)=\frac{K_0}{2}\alpha_3+\frac{K_M}{2}\alpha_3^3+\frac{K_F}{2}(\alpha_3^5-5\alpha_1^2\alpha_2^2\alpha_3)+\text{cubic anisotropy}; \tag{31}$$

$\tan^{-1}(1/\sqrt{2})<\theta<\pi/2$ and $\pi/2<\theta<\pi-\tan^{-1}(1/\sqrt{2})$:

$$F_{2,3}(T=0)=\frac{K_0}{2}(\alpha_1+\alpha_2\pm\alpha_3)+\frac{K_M}{2}(\alpha_1^3+\alpha_2^3\pm\alpha_3^3\pm3\alpha_1\alpha_2\alpha_3)+\frac{K_F}{2}(\alpha_1^5+\alpha_2^5\pm\alpha_3^5)+\alpha_1\alpha_2\alpha_3(\pm\alpha_1\alpha_2+\alpha_3+\alpha_1+\alpha_2\alpha_3)+\text{cubic anisotropy}; \tag{32}$$

$\pi-\tan^{-1}(1/\sqrt{2})<\theta<\pi$:

$$F_4(T=0)=-F_1(T=0)+\text{cubic anisotropy}, \tag{33}$$

where K_0 is given by a power series in η and has no effect on the resonance field,

$$K_M=\frac{NA}{12\sqrt{3}}\eta^3, \tag{34}$$

$$K_F=\frac{NA}{288\sqrt{3}}\eta^5, \tag{35}$$

and the cubic anisotropy is given by

$$K_{\rm cubic}=K_1(0)S+K_2(0)P, \tag{36}$$

$$S=\alpha_1^2\alpha_2^2+\alpha_1^2\alpha_3^2+\alpha_2^2\alpha_3^2, \tag{37}$$

$$P=\alpha_1^2\alpha_2^2\alpha_3^2, \tag{38}$$

$$K_1(0)=\left[\frac{5\sqrt{3}}{36}\eta^4+\frac{21\sqrt{3}}{36}\eta^6\right]N, \tag{39}$$

$$K_2(0)=\frac{7}{18}\eta^6N. \tag{40}$$

On the other hand, using Eqs. (20), (28), and (29), and dropping constant terms, we obtain the free energy at finite temperatures:

$$F(T)=-\frac{NkT}{4}\sum_{i=1}^{4}\ln\{1+\cosh[2\gamma(1+\eta\beta_{3,i})^{1/2}]+\cosh[2\gamma(1-\eta\beta_{3,i})^{1/2}]+\cosh[\gamma(1+\eta\beta_{3,i})^{1/2}]+\cosh[\gamma(1-\eta\beta_{3,i})^{1/2}]\},\tag{41}$$

where $\gamma=A/kT$. For $kT<A$, $F(T)$ is given by the zero-temperature expressions plus logarithmic (temperature-dependent) corrections. Therefore, for $kT<A$, including $T=0$, the free energy has noncubic components proportional to the cubic and fifth power of the magnetization components. For $kT>A$, however, the cubic symmetry is recovered:

$$F(T)=K_1(T)S+K_2(T)P,\tag{42}$$

where

$$K_1(T)=NkT\left[\frac{2}{9}\left(\frac{r}{q}\right)^2-\frac{4}{27}\left(\frac{r}{q}\right)^3+\frac{6}{81}\left(\frac{r}{q}\right)^4-\frac{8}{243}\left(\frac{r}{q}\right)^5\right],\tag{43}$$

$$K_2(T)=-NkT\left[\frac{16}{27}\left(\frac{r}{q}\right)^3-\frac{64}{81}\left(\frac{r}{q}\right)^4+\frac{160}{243}\left(\frac{r}{q}\right)^5\right],\tag{44}$$

$$r=\frac{17}{8}\gamma^4\eta^2,\tag{45}$$

$$q=5+5\gamma^2+\frac{17}{8}\gamma^4.\tag{46}$$

B. Cr^{3+} anisotropy

Using Eqs. (23a) and dropping constant terms, the ground-state energy for this ion on site i may be written as

$$E_{0,i}\equiv E_{3/2,i}=\left(\frac{3D}{2}-\frac{9D^2}{4\Delta E_x}-\frac{9D^3}{4\Delta E_x^2}\right)\beta_{3i}^2+\left(\frac{21D^2}{8\Delta E_x}-\frac{117D^3}{64\Delta E_x^2}\right)\beta_{3i}^4+\frac{135D^3}{32\Delta E_x^2}\beta_{3i}^6.\tag{47}$$

From Eq. (27) the free-energy contribution at $T=0$ K is thus obtained

$$F_a(T=0\ \text{K})=K_1S+K_2P,\tag{48}$$

where

$$K_1(T=0)=\left(\frac{7D^2}{6\Delta E_x}+\frac{5D^3}{2\Delta E_x^2}\right)N,\tag{49}$$

$$K_2(T=0)=\frac{15D^3}{2\Delta E_x^2}N.\tag{50}$$

For $T\neq 0$, using Eqs. (23) and Eqs. (28) and (29), the free energy for $kT<D$ reduces to the value at $T=0$ K plus exponential corrections in the form

$$F_{a,i}(T)=F_{a,i}(T=0)-\frac{NkT}{4}\sum_{i=1}^{4}\left\{\exp\left[-\frac{1}{kT}\left(\Delta E_x-3D\beta_{3i}^2-\frac{6D^2}{\Delta E_x}\beta_{3i}^4-\frac{135D^3}{16\Delta E_x^2}\beta_{3i}^6\right)\right]+\exp\left[-\frac{1}{kT}\left(2\Delta E_x-3D\beta_{3i}^2+\frac{3D^2}{4\Delta E_x}\beta_{3i}^4-\frac{135D^3}{16\Delta E_x^2}\beta_{3i}^6\right)\right]+\exp\left[-\frac{1}{kT}\left(3\Delta E_x-\frac{21D^2}{4\Delta E_x}\beta_{3i}^4\right)\right]\right\}.\tag{51}$$

For $kT>D$, the exponential terms can be expressed in power series. Dropping constant terms we obtain the following free energy:

$$F_a(T)=K_1S+K_2P,\tag{52}$$

where

$$K_1(T)=-\frac{NkT}{4}\left(\frac{16}{9}\chi_4+\frac{16}{9}\chi_6+\frac{32}{27}\chi_8\right)N,\tag{53}$$

$$K_2(T)=-\frac{NkT}{4}\left(\frac{64}{9}\chi_6+\frac{1024}{81}\chi_8\right)N,\tag{54}$$

$$\chi_4=-\frac{3D^2}{8kT\Delta E_x}\left(\frac{9F-7C}{A+B}\right)+9\left(\frac{D}{kT}\right)^2\frac{AB}{(A+B)^2},\tag{55}$$

$$\chi_6=-\frac{135D^3}{32kT\Delta E_x^2}\left(\frac{A-B}{A+B}\right)-\frac{9}{4}\left(\frac{D}{kT}\right)^3\left(\frac{A-B}{A+B}\right)+\frac{9D^3}{4\Delta E_x(kT)^2}\left(\frac{9FB+7CA}{A+B}\right),\tag{56}$$

$$\chi_8=-\frac{27D^4}{16(kT)^4}\left[\frac{1}{8}-\left(\frac{A-B}{A+B}\right)^2+\frac{3}{4}\left(\frac{A-B}{A+B}\right)^4\right]+\frac{9D^4}{64(kT)^2(\Delta E_x)^2}\left[\frac{139A+171B}{A+B}-\frac{1}{2}\left(\frac{9F-7C}{A+B}\right)^2-45\left(\frac{A-B}{A+B}\right)^2\right]+\frac{D^4}{64(kT)^3\Delta E_x}\left[\frac{-259C+333F}{A+B}+\frac{81}{8}\left(\frac{9FA+7CB}{A+B}\right)\left(\frac{A-B}{A+B}\right)\right],\tag{57}$$

$$A=\cosh\left(\frac{3\Delta E_x}{2kT}\right),\quad B=\cosh\left(\frac{\Delta E_x}{2kT}\right),\tag{58}$$

$$C=\sinh\left(\frac{3\Delta E_x}{2kT}\right),\quad F=\sinh\left(\frac{\Delta E_x}{2kT}\right).\tag{59}$$

C. Cr^{4+} anisotropy

For this ion we have to consider two cases according to the sign of the trigonal-field splitting.

1. Γ_3^- lowest ($\Delta_T>0$)

It is clear from the Eqs. (24) that the ground-state energy for this ion on site i is

$$E_{0,i}=-\lambda x\sqrt{1+\gamma^2+2\gamma|\beta_{3i}|}. \tag{60}$$

By defining $A=(\lambda x/2)\sqrt{1+\gamma^2}$ and $\eta=2\gamma/(1+\gamma^2)$, we observe that the above expression is similar to Eq. (20b) for the ground-state energy of the Cr^{2+} ion. The free-energy contribution at $T=0$ K is therefore identical to that previously obtained for the Cr^{2+} ions.

For $T\neq 0$ K the free-energy contributions have been derived using Eqs. (24) and (28) and (29). Dropping constants terms, we have

$$F_{a,i}(T)=-\frac{NkT}{4}\sum_{i=1}^{4}\ln[1+\cosh\tau(1+\eta\beta_{3i}) +\cosh\tau(1-\eta\beta_{3i})], \tag{61}$$

where $\tau=(\lambda x/kT)\sqrt{1+\gamma^2}$.

For $kT<\lambda x\sqrt{1+\gamma^2}$ this contribution reduces to the value at $T=0$ K, plus exponential corrections, as for the Cr^{2+} ions ($kT<A$). For $kT>\lambda x\sqrt{1+\gamma^2}$, similar expressions are also obtained as for the Cr^{2+} ions ($kT>A$), with the parameters in Eqs. (45) and (46) defined by

$$r=\frac{1}{8}\tau^4\eta^2 \quad \text{and} \quad q=3+\tau^2+\frac{\tau^4}{8}. \tag{62}$$

2. Γ_2^- lowest with $|\lambda|\approx|\Delta E_x|$

At $T=0$ K the four inequivalent site contributions add to a constant value. On the other hand, using Eqs. (25) and (28) and (29) and dropping constant terms, we obtain the free energy at finite temperatures:

$$F(T)=-\frac{NkT}{4}\sum_{i=1}^{4}\ln(1+X_i). \tag{63}$$

where

$$X_i=\frac{1}{2}\mathrm{sech}\left(\frac{\Delta E_x}{kT}\right)\exp\left[\frac{D}{2kT}(3\beta_{3i}^2-1)\right]. \tag{64}$$

For $kT>3D/2$ [see Eq. (26)], $\ln(1+X_i)$ and the exponential terms can be expressed in power series. Dropping constant terms, a cubic symmetry is recovered:

$$F(T)=K_1(T)S+K_2(T)P+K_3S^2, \tag{65}$$

$$K_1(T)=\frac{NkT}{2}\left[\frac{D^2\quad q}{(kT)^2(1-q)^2}\right], \tag{66}$$

$$K_2(T)=-NkT\left[\frac{D^3\quad q(q+1)}{(kT)^3(1-q)^3}\right], \tag{67}$$

$$K_3(T)=-\frac{NkT}{24}\left[\frac{D^2\quad q(q^2-7)}{(kT)^4\ (1-q)^4}\right], \tag{68}$$

$$q=\frac{1}{2}\mathrm{sech}\left(\frac{\Delta E_x}{kT}\right). \tag{69}$$

VI. MICROSCOPIC INTERPRETATION OF THE EXPERIMENTAL DATA AND CONCLUSIONS

In the last two sections we have calculated the energy levels and the single-ion contributions to the anisotropy associated with the Cr^{2+}, Cr^{3+}, and Cr^{4+} ions present in the spinel chalcogenides. The more relevant results of the calculations can be summarized as follows: (i) crossovers of the two low-lying energy levels of the Cr^{2+} ions occur in the [112] direction at site γ_1, in the [110] direction at sites γ_2 and γ_3, and in the [112] direction at site γ_4 [see Fig. 12(b)]. On the other hand, near crossings occur in the [100] direction at the four lattice sites for both the Cr^{2+} and Cr^{4+} ($\Delta_T<0$) ions [Figs. 12(b) and 14(b)]. Near crossings of the two low-lying energy levels of the Cr^{4+} ($\Delta_T<0$) ions occur also in the [111] direction at site γ_1, and in direction [111] at site γ_4 [Fig. 14(b)]. (ii) As a result of the doublet orbital ground state of the Cr^{2+} ions and the level crossings, we find that a symmetry breaking of the anisotropy from cubic, at high temperatures, to noncubic at low temperatures occurs. (iii) The Cr^{3+} ions produce a small cubic anisotropy, $K_1, K_2>0$, which play a significant role only in the almost perfect stoichiometric sample. (iv) The single-ion contribution of the Cr^{4+} ions to the anisotropy is also cubic. For $\Delta_T>0$, we find that $K_1>0$, $K_2<0$, and $K_3>0$, whereas for $\Delta_T<0$, $K_1, K_2<0$ and $K_3>0$.

In FMR experiments, for an applied magnetic field in the (110) plane, the salient feature of the noncubic component of the anisotropy, according to the result (ii) above, is the asymmetry of the resonance field $H_{\mathrm{res}}(\theta)$ about the [110] direction, a ''signature'' of the presence of Cr^{2+} ions in the system. In Fig. 15 we report FMR data for the angular dependence of the $H_{\mathrm{res}}(\theta)$ of single crystals of $CdCr_2Se_4$ with 0.1 mole% Ag at $T=4.2$ K, where this effect is seen. For this sample of relatively low conductivity (see Fig. 6) only the uniform mode is excited and thus a good fitting of the data is obtained using Kittel's condition, Eq. (1), including also appropriated effective anisotropic demagnetizing factors through Eqs. (9)–(10). Regardless the Ag doping, the contribution of Cr^{2+} ions is sizable, probably due to the large amount of Se defects. The asymmetry of the $H_{\mathrm{res}}(\theta)$ about the [110] direction has been observed[6–8] in several FMR studies of both $CdCr_2Se_4$ and $CdCr_2S_4$, but either ignored or attributed[6] to a small deviation from sample sphericity. However, this could not produce such a big effect, which has in fact an intrinsic origin as explained above. In Fig. 15 we present also a fitting of the data, where the discontinuities in the theoretical curve reflect the level-crossing approximation used to calculate $H_{\mathrm{res}}(\theta)$ from Eqs. (7) and (9). We have used the $T=0$ expressions for the free energy, Eqs. (31)–(33), since at 4.2 K the logarithmic corrections are negligible.

It is clear that the asymmetry of the $H_{\mathrm{res}}(\theta)$ is justified by the presence of Cr^{2+} ions, in agreement with the theoretical results derived in Sec. V. Though we do not have a complete

TABLE I. Experimental and theoretical estimates for the cubic anisotropy constants in 1.3 mole% Ag-doped $HgCr_2Se_4$ for various temperature values.

	K_1 (cm^{-1}/ion)		K_2 (cm^{-1}/ion)		K_3 (cm^{-1}/ion)	
T (K)	Expt.	Theory	Expt.	Theory	Expt.	Theory
15	−2.68	−1.26	−10.57	−2.31	5.27	0.87
30	−1.97	−2.06	−7.45	−4.07	3.42	0.59
45	−1.58	−1.95	−5.99	−2.97	2.88	0.40
60	−1.17	−1.66	−4.14	−2.05	2.02	0.16
75	−0.82	−1.45	−3.03	−1.44	1.47	0.10
90	−0.60	−1.25	−2.01	−1.04	0.99	0.06
110	−0.22	−1.06	−0.67	−0.73	0.33	0.03

knowledge of the parameters involved, we can test the consistency of the values of the anisotropy constants obtained from the fitting of the data in Fig. 15. Indeed K_M and K_F were found to be negative, in accord with the sign[32] of the cubic crystal-field splitting Δ. Also, K_F is smaller than K_M as predicted by Eqs. (34) and (35). Taking[32] $\lambda = 58$ cm^{-1}, $(v/\Delta) \simeq (-1/10)$, and assuming a typical concentration of 10^{19} Cr^{2+} ions per cm^3, we find $\Delta E_x \simeq 70$ cm^{-1}, which is the correct order of magnitude for the exchange energy since the observed asymmetry persists in the entire ferromagnetic region. On the other hand, from the values of K_1 and K_2, we conclude that a complete explanation of the cubic component requires including the contributions from the Cr^{4+} and Cr^{3+} ions.

The simultaneous contributions of Cr ions of different valences to the 0.1 mole% Ag-doped $CdCr_2Se_4$ anisotropy and FMR relaxation forbid the possibility of a quantitative analysis of our results for the H_{res} and ΔH maxima as shown in Fig. 7. In spite of this, our results for the low-lying energy levels of the Cr^{2+} and Cr^{4+} ions suggest that the fast relaxation mechanism due to Cr^{4+} ions is responsible for the ΔH maxima along the [100] and [111] directions at low temperatures. The ΔH maxima along the [110] is probably associated with a relaxation mechanism due to Cr^{2+} ions which shows level crossing along this direction. The two peaks of ΔH in the [100] direction at higher temperatures may be due to the slow relaxation of Cr^{4+} ions or due to the valence exchange mechanism of Cr^{2+}-Cr^{3+} or Cr^{3+}-Cr^{4+}.

Since we find that the $H_{res}(\theta)$ curves for ''as grown'' $HgCr_2Se_4$ and 1.3 mole% Ag-doped $CdCr_2Se_4$ are symmetrical about the [110] direction, we conclude, in agreement with result (ii) above that there is no substantial amount of Cr^{2+} ions in these samples. The fitting of these curves predicts $K_1 < 0$, and should accordingly [see result (iv) above] be ascribed to the presence of Cr^{4+} ions. The presence of these ions shows up more conclusively in the temperature dependence of ΔH for 1.3 mole% Ag-doped $CdCr_2Se_4$ (Fig. 9), in which case a fast relaxation mechanism due to Cr^{4+} ions is responsible for the peak along the [100] direction at low temperatures [see result (i)], with a relaxation time $\tau_0 = 3.3 \times 10^{-13}$ s and [using Eqs. (25)] an exchange field between these ions and the host Cr^{3+} ions of $\Delta E_x = 16.7$ cm^{-1}. On the other hand, for ''as grown'' $HgCr_2Se_4$ (Figs. 8 and 10) a slow relaxation mechanism due to Cr^{4+} ions with $\Delta E_x = 16.0$ cm^{-1} and $\tau_0 = 1.8 \times 10^{-11}$ s fits the data nicely. The fitting for the [111] direction was obtained using Eqs. (25) and assuming a statistical distribution over the distinct B sites. From this fitting we obtained the additional parameter $D = 9.0$ cm^{-1}. The difference of the exchange fields ΔE_x may be accounted for by the distinct transition temperatures of the two compounds. However, the two order of magnitude difference of the relaxation times (fast and slow) from one compound to another is a striking example of the complex behavior of impurity magnetic ions in spinel magnetic semiconductors.

The $H_{res}(\theta)$ curves for 1.3 mole% Ag-doped $HgCrSe_4$ (see Fig. 3) for temperatures in the entire ferromagnetic region are symmetrical about the [110] direction and therefore we conclude also that no substantial amount of Cr^{2+} ions is present in this case. At all temperatures, the fittings predict $K_1, K_2 < 0$ and $K_3 > 0$ and should accordingly be ascribed to the presence of Cr^{4+} ions (case $\Delta_T < 0$). The first three anisotropy constants are in reasonable quantitative agreement if we assume the concentration of 4.5×10^{20} Cr^{4+} ions/cm^3 (nominal concentration of Ag) and reliable values for the parameters of this ion in ''as grown'' $HgCr_2Se_4$ crystal obtained by the relaxation mechanism analysis ($\Delta E_x = 16.0$ cm^{-1} and $D = 9.0$ cm^{-1}). The results are displayed in Table I.

Our results and discussion concerning the effect of magnetic impurity ions on the FMR linewidth and anisotropy complement those reported in Secs. II and III, where we have studied the dependence of the FMR line shape and linewidth on the sample conductivity, as well as the temperature dependence of the linewidth on the two-magnon relaxation mechanism. In particular, we have shown that while in the sample of low conductivity only the uniform mode is excited in a FMR experiment, in those having high enough conductivity the resonance condition is associated with the excitation of a spin-wave manifold in a regime where exchange effects are irrelevant and characterized by a quite asymmetrical FMR line shape.

In Secs. III and IV crystal-field theory was used to calculate the Cr ions low-lying energy levels and their effect on the magnetic anisotropy and FMR relaxation. We showed that the orbital ground state of the Cr^{2+} ion is a doublet and causes a symmetry breaking of the anisotropy from cubic, at high temperatures, to noncubic at low temperatures. In this section we reported FMR data of a single crystal of

$CdCr_2Se_4$ with 0.1 mole% Ag doped where this effect is seen. Moreover, several relaxation mechanisms were identified, which allowed the estimates of exchange fields and microscopic relaxation times of Cr ions in these crystals.

In conclusion, our analysis of the reported theoretical and experimental results have shown that the chalcogenide spinels are very interesting magnetic systems and offer many possibilities of studying the interplay between magnetic and electrical properties, as well as striking effects due to the presence of impurity magnetic ions in these compounds.

ACKNOWLEDGMENTS

We thank P. Gibart and S. M. Rezende for fruitful discussions and collaboration in several stages of this work. Financial support from CNPq and FINEP (Brazilian agencies) are gratefully acknowledged.

[1] P. K. Baltzer, H. W. Lehmann, and M. Robbins, Phys. Rev. Lett. **15**, 493 (1965); P. K. Baltzer, P. J. Wojtowicz, M. Robbins, and E. Lopatin, Phys. Rev. **151**, 367 (1966). See, also, E. L. Nagaev, *Physics of Magnetic Semiconductors* (MIR, Moscow, 1983).

[2] R. C. LeCraw, H. von Phylipsborn, and M. D. Sturge, J. Appl. Phys. **38**, 965 (1967).

[3] H. W. Lehmann and M. Robbins, J. Appl. Phys. **37**, 1389 (1966); V. A. Kostylev, B. A. Gizhevskil, A. A. Samokhvalov, and N. M. Chebotaev, Sov. Phys. Solid State **32**, 20 (1990).

[4] A. A. Samokhvalov, N. I. Solin, N. A. Viglin, V. A. Kostylev, V. V. Osipov, and V. S. Babushkin, Phys. Status Solidi B **169**, K93 (1992).

[5] M. Lubecka and L. J. Maksymowicz, Phys. Rev. B **44**, 10 106 (1991), and references therein.

[6] A. G. Gurevich, Ju. M. Jacovlev, V. I. Karpovich, A. N. Ageev, and E. V. Rubalskaja, Phys. Lett. **40A**, 69 (1972); I. G. Botsan, V. I. Zheru, S. I. Radautsan, S. A. Ratseev, and V. E. Tézlévan, Sov. Phys. Solid State **31**, 2001 (1989); K. G. Nikiforov, M. Baran, V. K. Belyaev, L. Ya. Pasenko, S. I. Radautsan, and A. Wisniewski, Phys. Status Solidi B **158**, K63 (1990).

[7] S. B. Berger and H. L. Pinch, J. Appl. Phys. **38**, 949 (1967); H. L. Pinch and S. B. Berger, J. Phys. Chem. Solids **29**, 2091 (1968).

[8] B. Hoekstra and R. P. van Stapele, Phys. Status Solidi B **55**, 607 (1973).

[9] B. Hoekstra, R. P. van Stapele, and A. B. Voermans, Phys. Rev. B **6**, 2762 (1972).

[10] A. I. Bairamov, A. G. Gurevich, V. I. Karpovich, V. T. Kalinnikov, T. G. Aminov, and L. M. Émiryan, Sov. Phys. Solid State **18**, 396 (1976).

[11] A. I. Bairamov, A. G. Gurevich, L. M. Émiryan, and N. N. Parfenova, Sov. Phys. Solid State **19**, 1563 (1977).

[12] J. M. Ferreira and M. D. Coutinho-Filho, J. Phys. (Paris) Colloq. **39**, C6-1007 (1978).

[13] L. M. Émiryan, A. G. Gurevich, A. S. Shukyurov, and V. N. Berzhanskii, Sov. Phys. Solid State **23**, 1700 (1981); N. I. Solin, A. A. Samokhvalov, I. Yu. Shumilov, S. V. Naumov, and N. M. Chebotaev, *ibid*. **30**, 1260 (1988); K. G. Nikiforov, A. G. Gurevich, L. Ya Pasenko, S. I. Radautsan, and L. M. Emiryan, Phys. Status Solidi A **116**, K185 (1989). The study of the influence of annealing in vacuum, in Se vapor and in Hg vapor, was reported by K. G. Nikiforov, A. G. Gurevich, L. Ya. Pasenko, S. I. Radautsan, and L. M. Émiryan, Sov. Phys. Solid State **27**, 1452 (1985).

[14] J. M. Ferreira and M. D. Coutinho-Filho, J. Magn. Magn. Mater. **54-57**, 1280 (1986).

[15] H. Oudet, P. Gibart, M. Porte, T. Merceron, and G. Villers (unpublished).

[16] J. M. Ferreira, M. D. Coutinho-Filho, and S. M. Rezende, Solid State Commun. **62**, 159 (1987).

[17] N. A. Viglin, A. A. Samakhvalov, N. I. Solin, and M. I. Simonova, Sov. Phys. Solid State **26**, 749 (1984).

[18] See, e.g., V. K. Belyaev, K. G. Nikiforov, S. I. Radautsan, and V. A. Bazakutsa, Cryst. Res. Technol. **24**, 371 (1989), and references therein.

[19] *Ferromagnetic Resonance*, edited by S. V. Vonsovskii (Pergamon, Oxford, 1966).

[20] See, e.g., D. S. Rodbell, in *Resonance and Relaxation in Metals*, edited by F. L. Vogel, Jr. (Plenum, New York, 1964); Phys. Rev. Lett. **13**, 471 (1964); R. E. Prange and V. Korenman, J. Magn. Reson. **6**, 274 (1972).

[21] W. S. Ament and G. T. Rado, Phys. Rev. **97**, 1558 (1955).

[22] Y. Watanabe, S. Saito, and M. Marysko, J. Magn. Magn. Mater. **50**, 239 (1985).

[23] J. M. Ferreira, M. D. Coutinho-Filho, S. M. Rezende, and P. Gibart, J. Magn. Magn. Mater. **31-34**, 672 (1983).

[24] S. Saito, S. Takemoto, and Y. Watanable, Phys. Status Solidi A **34**, 671 (1976), and references therein.

[25] A. G. Gurevich, Sov. Phys. Solid State **16**, 1159 (1974); M. Marysko, Phys. Status Solidi A **28**, K159 (1975); J. M. Ferreira and M. D. Coutinho-Filho, Solid State Commun. **28**, 775 (1978); N. A. Viglin, A. A. Samokhvalov, N. M. Chebotaev, and B. A. Gizhevskii, Sov. Phys. Solid State **30**, 1042 (1988).

[26] See, e.g., J. H. Van Vleck, J. Appl. Phys. **35**, 882 (1964); M. Sparks, *ibid*. **38**, 1031 (1967); A. G. Gurevich, A. N. Ageev, and M. T. Klinger, *ibid*. **41**, 1295 (1970); M. A. Vinnik, E. V. Rubal'skaya, and Yu. M. Yakovlev, Bull. Acad. Sci. USSR, Phys. Ser. **39**, 176 (1975).

[27] A. I. Bairamov, A. G. Gurevich, L. A. Émiryan, and N. N. Parfenova, Phys. Lett. **62A**, 242 (1977); A. G. Gurevich, Sov. Phys. Solid State **16**, 1159 (1984).

[28] H. W. Lehmann, Phys. Rev. **163**, 488 (1967).

[29] N. Kamata, S. Yamazaki, S. Kabashima, T. Hattanda, and T. Kawakubo, Solid State Commun. **10**, 905 (1972).

[30] K. Kashi, P. Kuivalainen, T. Salo, H. Stubb, and T. Stubb, in *Magnetism and Magnetic Materials*, edited by J. J. Becker and G. H. Lander, AIP Conf. Proc. No. 34 (AIP, New York, 1976), p. 187; N. I. Solin, A. A. Samokhvalov, and B. A. Gizhevskii, Sov. Phys. Solid State **19**, 375 (1977).

[31] J. C. Slonczewski, J. Appl. Phys. **32**, 253S (1961).

[32] See, e.g., A. Abragam and B. Bleaney, *Electron Paramagnetic Resonance of Transition Ions* (Clarendon, Oxford, 1970).

[33] See, e.g., R. M. White, *Quantum Theory of Magnetism* (McGraw-Hill, New York, 1970), Chap. 2.